To appear in: **Majlesi Journal of Electrical Engineering (MJEE)**

Online ISSN: 2345-377X **Print ISSN:** 2345-3796

Received: 31- Aug-2025

Revised: 26-Nov-2025

Accepted: 01-Jan-2026

DOI: 10.57647/mjee.2026.2002.15

Original Research

A Real-Time Driver Drowsiness Detection Method Using a Hybrid of Deep Learning and Fuzzy Logic

Amir Sohrabinezhad[1], Reza Sabbaghi-Nadooshan[1,*], Nasser Talebi[2], Roohollah. Barzamini[1], Fardad Farokhi[3]

1- Department of Electrical Engineering, CT.C, Islamic Azad University, Tehran, Iran.
Email: amir.sohrabinezhad@iau.ac.ir, r_sabbaghi@iau.ac.ir, r.barzamini.eng@iau.ac.ir
2- Department of Electrical Engineering, YI.C, Islamic Azad University, Tehran, Iran.
Email: n.talebi@iau.ac.ir
3- Department of Biomedical Engineering, CT.C, Islamic Azad University, Tehran, Iran.
Email: f_farokhi@iauctb.ac.ir

ORCID iDs: Amir Sohrabinezhad https://orcid.org/0009-0000-5491-5079
Reza Sabbaghi-Nadooshan https://orcid.org/0000-0003-1201-914X
Nasser Talebi https://orcid.org/0000-0002-4183-2861
Roohollah Barzamini https://orcid.org/0000-0002-4892-3723
Fardad Farokhi https://orcid.org/0000-0002-6045-5424

Abstract

Driver drowsiness contributes to approximately 21% of traffic accidents. Three deep neural networks were trained, with ResNet50 achieving the best performance: 99.74% training accuracy, 99.62% validation accuracy, an average test F1-score of 0.99, no overfitting, and real-time inference at 0.023 seconds per frame on an RTX 3060 laptop GPU with 6GB RAM. Following drowsiness detection, a fuzzy inference system integrating Eye Aspect Ratio (EAR) and Mouth Aspect Ratio (MAR) is applied to determine the drowsiness severity. The system was tested with an infrared camera on 453 volunteers from various Middle Eastern ethnic groups under different lighting conditions. A local database was compiled from these tests, recording 31 misclassifications and achieving an overall accuracy of 93.16%. The findings demonstrate that the system performs reliably under both day and night conditions and across diverse ethnicities, supporting its suitability for integration into advanced driver-assistance systems (ADAS).

Keywords: Real-time Drowsiness Detection, Determining the degree of drowsiness, Deep Learning, Fuzzy Inference Systems.

1. Introduction

Drowsiness is a leading factor in road accidents, causing significant human and economic losses. To address this issue, advanced approaches such as deep neural networks, machine learning algorithms, and intelligent paradigms like fuzzy logic have been applied, all with the objective of improving real-time detection accuracy and activating in-vehicle audio alerts to keep

drivers awake. The present study integrates intelligent techniques with large-scale field testing to deliver comprehensive results. Beyond detection accuracy, the system also evaluates frame-level real-time processing performance, enabling a joint assessment of both speed and precision. One common implementation strategy for drowsiness detection systems utilizes convolutional neural networks (CNNs), such as VGG16 [1], one of the effective approaches in training deep neural networks is the use of transformer-based architectures, which offer highly favorable accuracy and performance [2, 3], a**s** well as other architectures [4–15], which have shown high accuracy rates. A traditional PERCLOS-based method was also employed for drowsiness detection [16]. Eye closure and yawning detection are implemented using the dlib library and Python [17, 18]. Both dlib and OpenCV are widely employed in Python-based driver monitoring systems [19]. Research indicates that around 21% of all road accidents are associated with driver fatigue. To improve image quality and detection performance, Support Vector Machine (SVM) classifiers and Histogram of Oriented Gradients (HOG) features are often combined with dlib and OpenCV frameworks [20]. Validation is performed through live video streams and dedicated databases [21]. Further improvements to the traditional convex hull algorithm have been proposed via advanced filtering methods [22]. Additionally, facial feature localization is achieved through machine learning-based recognition of 68 key landmarks [23, 24]. Fuzzy logic is then applied to interpret eye activity, providing an estimation of drowsiness levels [25–28]. Fuzzy logic is employed in various systems characterized by uncertainty in categorized values [29-33]. One specialized domain where fuzzy logic proves particularly effective is image processing [34-37].

2. Proposed Method

At the initial stage, three neural networks were trained on a drowsiness dataset containing two labels: *Normal* and *Drowsiness*. A performance comparison was carried out among these networks and findings from related studies. The most suitable network was selected based on training accuracy, validation outcomes, test performance, and real-time inference capability on an RTX 3060 laptop GPU with 6GB RAM. The chosen model was then integrated with an image processing approach utilizing Eye Aspect Ratio (EAR) and Mouth Aspect Ratio (MAR) features, combined with a fuzzy logic system to estimate the degree of driver drowsiness. The developed system was validated in field experiments with 453 participants of diverse ethnic origins from the Middle East. Live camera testing confirmed the reliability of the proposed framework. The complete block diagram of the system is presented in Fig. 1, while the recommended in-vehicle camera installation point is depicted in Fig. 2-a**.** An image captured from this installation position is shown in Fig. 2-b**.**

The research gaps identified through the review of similar studies highlight the necessity of conducting this research (Table 1). The combination of the model trained with the ResNet50 deep neural network, together with EAR/MAR-based fuzzy inference and its validation on 453 volunteers in live tests, demonstrated that the proposed hybrid method effectively addresses the gaps left by previous approaches.

2.1. Convolutional Neural Networks for Drowsiness Detection

For the implementation of all neural networks in this study, a publicly available and free drowsiness dataset was utilized, accessible at:

(https://universe.roboflow.com/ltomic01/driver-drowsiness-detection-gk0ws/dataset/1/download).

This dataset, divided into two categories with class labels Normal and Drowsiness, was used for training, validation, and testing. The original image dimensions were 640×640 pixels, and all images were resized to 224×224 pixels before being fed into the networks. Model training was conducted on an RTX 3060 laptop GPU with 6 GB of RAM. The initial configuration parameters for each network are summarized in Table 2. The default number of training epochs for all neural

networks used in this study was set to 50. However, a common condition was applied for all three networks: if the training results became stable and repetitive, training would be stopped. Consequently, the ResNet50 neural network was trained for only 23 epochs, while the ViT-Tiny network completed 13 training epochs. The specifications of the dataset used, along with the applied configurations, are presented in Table 3.

The collected dataset obtained from the field tests was captured using a camera whose technical specifications are presented in Table 4. The distance between the camera and the subject during field testing and database collection was set between 30 and 80 centimeters to ensure that the camera and the system could be installed in vehicles of various sizes.

A computer vision system is considered real-time if it processes each video frame within a time less than or equal to the interval between two consecutive frames, satisfying the real-time constraint (Equation 1).

$$\begin{cases} T_{inference} \le \Delta t \\ \Delta t = \dfrac{1}{f_{fps}} \end{cases} \Rightarrow T_{inference} \le \frac{1}{f_{fps}} \qquad (1)$$

$T_{inference}$: Time to process one frame (inference time)

Δt : Time between two frames

f_{fps} : Frame rate of the video (frames per second)

Given that 25 frames per second are received from the camera for processing, each frame therefore requires 0.04 seconds to be processed. This duration represents the maximum time that can be considered as the real-time threshold.

$$T_{inference} \le \Delta t \Rightarrow T_{inference} \le \frac{1}{25} = 0.04s$$

The F1-score was calculated based on the validation set using the standard definition to assess the neural network's classification performance (Equation 2) [3, 11].

$$F1 - Score = 2 \times \frac{Precision \times Recall}{Precision + Recall} \qquad (2)$$

The resulting F1-Score is always a number between 0 and 1. A value close to 0 indicates that the model performed poorly, while a value close to 1 indicates that the model was accurate and missed very few cases.

In the first supervised training, performed using the ResNet-50 network, the model was trained with the Adam optimizer and the cross-entropy loss function. The network was trained for 23 epochs, achieving an average training accuracy of 99.74% and an average validation accuracy of 99.62% (Fig 3). In the real-time inference processing test, an average processing time of 0.023 seconds per frame was obtained, indicating that the processing was performed within the real-time range on the GPU (Fig 4).

In the second supervised training, conducted using the MobileNetV3 network, the network was trained for 50 epochs, achieving an average training accuracy of 99.08% and an average validation accuracy of 96.84% (Fig 5). In the real-time inference processing test, an average processing time of 0.021 seconds per frame was obtained, indicating that the processing was not performed within the real-time range on the GPU (Fig 6).

In the third supervised training, conducted using the vit-tiny network, the network was trained for 13 epochs, achieving an average training accuracy of 98.62% and an average validation accuracy of 98.46% (Fig 7). In the real-time inference processing test, an average processing time of 0.020 seconds for most frames and up to 0.022 seconds for some frames was obtained, indicating that the processing was not performed within the real-time range on the GPU (Fig 8).

The three neural networks examined in this study demonstrate differences in performance. The evaluation results, along with the corresponding output charts, are presented to illustrate the models' accuracy (Figs. 9, 10, 11).

The comparative analysis of ResNet50 performance on the training and validation datasets, as shown in Fig. 9, highlights the model's strong generalization capability. The training accuracy is 99.74%, while the validation accuracy is 99.62%, indicating that the model effectively learns discriminative features without significant overfitting. Similarly, the precision, recall, and F1-score for both datasets are nearly identical and all reach approximately 99%. This balanced performance across the evaluation metrics demonstrates that the model is equally effective in minimizing false positives and false negatives, thereby providing reliable detection of both drowsy and normal states. The negligible gap between training and validation performance further confirms the model's robustness when exposed to unseen data. Such stability is particularly important for safety-critical applications such as driver monitoring, where both sensitivity to drowsiness and avoidance of false alarms are essential. Overall, these results validate ResNet50 as a dependable and well-generalized architecture for real-time driver drowsiness detection (Fig. 9).

The comparative performance analysis of MobileNetV3-Small on the training and validation datasets, as illustrated in Fig. 10, highlights the model's strong generalization capability. The training accuracy is 99.08%, while the validation accuracy is 96.84%, which shows a noticeable decrease compared to the validation accuracy achieved by the ResNet50 neural network. Similarly, the precision, recall, and F1-score metrics exhibit identical and closely matched values for both datasets. The recall value is 96%, and the precision value is 97%, and the F1-score is 96.49%. This nearly balanced performance across all metrics indicates that the model is equally effective in reducing false positives and false negatives; however, it does not ensure as reliable discrimination between drowsy and normal states as the ResNet50 network (Fig. 10).

The comparative performance analysis of ViT-Tiny on the training and validation datasets, as illustrated in Fig. 11, highlights the model's strong generalization capability. The training accuracy is 98.62%, while the validation accuracy is 98.46%, indicating a slight decrease compared to the validation accuracy achieved by the ResNet50 neural network. Similarly, the precision, recall, and F1-score metrics exhibit nearly identical values across both datasets. The recall is 98%, the precision is 98%, and the F1-score is 98%. This nearly balanced performance across all metrics demonstrates that the model is equally effective in reducing false positives and false negatives; however, it does not guarantee as reliable discrimination between drowsy and normal states as the ResNet50 network (Fig. 11).

At the conclusion of the evaluation of the selected neural networks in this study, confusion matrix figures (Figs. 12, 13, and 14) were added for the trained hybrid model systems, illustrating the distribution of true positives, false positives, true negatives, and false negatives. These figures provide clearer insight into the types of errors observed during the validation of each model.

The confusion matrix of the ResNet50 model clearly illustrates its classification performance. Out of a total of 289 test samples, the model correctly identified 144 drowsy cases and 143 normal cases. One drowsy sample was incorrectly classified as normal (false negative), and one normal sample was incorrectly classified as drowsy (false positive). Overall, the network demonstrates very high accuracy (Fig. 12).

The confusion matrix of the MobileNetV3-Small model clearly illustrates its classification performance. Out of a total of 289 test samples, the model correctly identified 139 drowsy cases and 140 normal cases, while 6 drowsy samples were incorrectly classified as normal (false negatives) and 4 normal samples were incorrectly classified as drowsy (false positives). These statistics indicate that, compared to the ResNet50 model, this network exhibits a higher number of classification errors (Fig. 13).

The confusion matrix of the ViT-Tiny model clearly illustrates its classification performance. Out of a total of 289 test samples, the model correctly identified 142 drowsy cases and 141 normal cases, while 3 drowsy samples were incorrectly classified as normal (false negatives) and 3 normal samples were incorrectly classified as drowsy (false positives). These statistics indicate that, compared to the ResNet50 model, this network exhibits a slightly higher number of classification errors (Fig. 14).

2.2. Drowsiness Level Assessment

The “shape_predictor_68_face_landmarks.dat” dataset was employed to extract 68 facial landmarks (Fig. 15 and Table 5). Using these landmarks, the Eye Aspect Ratio (EAR) and Mouth Aspect Ratio (MAR) metrics were calculated to measure eye closure and mouth opening, respectively, for estimating the severity of drowsiness (Equation 3). This approach introduces two primary challenges. The first challenge is normal blinking, where certain individuals naturally exhibit a higher frequency or longer duration of eyelid closure, which may be misinterpreted as drowsiness. The second challenge arises when the driver engages in conversation with passengers, as mouth movements during speech can resemble yawning, potentially leading to false detections. To mitigate these issues, the Mamdani fuzzy inference method was integrated with EAR and MAR analysis in this study. A further challenge is the variability of facial features among individuals from different ethnic groups. To overcome this, extensive field tests were conducted across diverse ethnic populations, generating a localized database from real-world experiments. The outcomes of these comprehensive tests validated the robustness and high accuracy of the proposed system.

$$\begin{cases} EAR_{Right\_eye} = \dfrac{\|P_{38}-P_{42}\|+\|P_{39}-P_{41}\|}{2\|P_{37}-P_{40}\|} \\ EAR_{left\_eye} = \dfrac{\|P_{44}-P_{48}\|+\|P_{45}-P_{47}\|}{2\|P_{43}-P_{46}\|} \end{cases}$$

$$\Rightarrow EAR = \left(\frac{EAR_{Right\_eye} + EAR_{Left\_eye}}{2}\right)$$

$$\begin{cases} \begin{cases} M_1 = P_{49} \\ M_8 = P_{55} \end{cases} \\ Average_{Upper\_lip} = \left\{ M_3 = \dfrac{|P_{51}-P_{62}|}{2},\ M_5 = \dfrac{|P_{52}-P_{63}|}{2},\ M_7 = \dfrac{|P_{53}-P_{64}|}{2} \right. \\ Average_{Lower\_lip} = \left\{ M_2 = \dfrac{|P_{57}-P_{66}|}{2},\ M_4 = \dfrac{|P_{58}-P_{67}|}{2},\ M_6 = \dfrac{|P_{59}-P_{68}|}{2} \right. \end{cases} \quad (3)$$

$$\Rightarrow MAR = \frac{\|M_3-M_2\|+\|M_5-M_4\|+\|M_7-M_6\|}{3\|M_1-M_8\|}$$

The membership functions of the fuzzy variables EAR and MAR were defined to describe their degrees of membership (Equation 4), while the resulting fuzzy membership functions from the combined EAR and MAR rules were derived based on these definitions (Equation 5). Taking into account the driver's eye condition—classified into three states: open, closed, and semi-closed—and the mouth condition—classified as closed, open, and semi-open—three fuzzy membership functions were defined for the eyes and three for the mouth. By combining these membership functions and formulating fuzzy rules, nine unique states were established, providing a complete set of rules for assessing the driver's drowsiness level. The parameters of these membership functions were determined based on regular partitioning and practical experience (Equations 4 and 5). Validation of the fuzzy inference results using sensitivity analysis indicates the high accuracy of the selected membership function parameters.

$$\mu_{EAR(Closed\,eye)}(x): \begin{cases} 1 & 0 \le x \le 0.2 \\ 1-x & 0.2 < x < 0.5 \\ 0 & 0.5 \le x \le 1 \end{cases},\ \mu_{EAR(Semi\,Closed)}(x): \begin{cases} 0 & 0 \le x \le 0.2 \\ x+1 & 0.2 < x < 0.5 \\ 1-x & 0.5 \le x < 0.8 \\ 0 & 0.8 \le x \le 1 \end{cases}$$

$$\mu_{EAR(Open)}(x): \begin{cases} 0 & 0 \le x \le 0.5 \\ x+1 & 0.5 < x < 0.8 \\ 1 & 0.8 \le x \le 1 \end{cases},\ \mu_{MAR(Normal)}(x): \begin{cases} 1 & 0 \le x \le 5 \\ 1-x & 5 < x < 15 \\ 0 & 15 \le x \le 30 \end{cases} \quad (4)$$

$$\mu_{MAR(medium)}(x): \begin{cases} 0 & 0 \le x \le 5 \\ x+1 & 5 < x < 15 \\ 1-x & 15 < x < 25 \\ 0 & 25 \le x \le 30 \end{cases},\ \mu_{MAR(yawn)}(x): \begin{cases} 0 & 0 \le x \le 15 \\ x+1 & 15 < x < 25 \\ 1 & 25 \le x \le 30 \end{cases}$$

Mamdani fuzzy rules for determining the level of drowsiness by combining EAR and MAR:

Considering that three fuzzy membership functions were defined for EAR and three for MAR, representing the driver's eye closure and mouth status respectively, the combination of these two sets of membership functions resulted in a maximum of nine fuzzy rules.

1.Rule 1: If EAR is Closed and MAR is Normal, then the drowsiness level is asleep.
2.Rule 2: If EAR is Closed and MAR is yawning, then the drowsiness level is very high (vh).
3.Rule 3: If EAR is Closed and MAR is medium, then the drowsiness level is high (h).
4.Rule 4: if EAR is semi closed and MAR is yawning, then drowsiness level is medium high (mh).
5.Rule5: if EAR is semi closed and MAR is medium, then the drowsiness level is medium (m).
6.Rule 6: if EAR is semi closed and MAR is Normal, then the drowsiness level is medium low (ml).
7.Rule 7: if EAR is open and MAR is yawning, then the drowsiness level is low (l).
8.Rule 8: if EAR is open and MAR is medium, then the drowsiness level is very low (vl).
9.Rule 9: if EAR is open and MAR is Normal, then the drowsiness level is awake (a).

$$\mu_a(x):\begin{cases}1 & 0\le x\le 0.1\\ 1-x & 0.1<x<0.2\\ 0 & 0.2\le x\le 1\end{cases},\ \mu_{vl}(x):\begin{cases}0 & 0\le x\le 0.1\\ x+1 & 0.1<x<0.2\\ 1-x & 0.2\le x<0.3\\ 0 & 0.3\le x\le 1\end{cases},$$

$$\mu_l(x):\begin{cases}0 & 0\le x\le 0.2\\ x+1 & 0.2<x<0.3\\ 1-x & 0.3\le x<0.4\\ 0 & 0.4\le x\le 1\end{cases},\ \mu_{ml}(x):\begin{cases}0 & 0\le x\le 0.3\\ x+1 & 0.3<x<0.4\\ 1-x & 0.4\le x<0.5\\ 0 & 0.5\le x\le 1\end{cases},$$

$$\mu_m(x):\begin{cases}0 & 0\le x\le 0.4\\ x+1 & 0.4<x<0.5\\ 1-x & 0.5\le x<0.6\\ 0 & 0.6\le x\le 1\end{cases},\ \mu_{mh}(x):\begin{cases}0 & 0\le x\le 0.5\\ x+1 & 0.5<x<0.6\\ 1-x & 0.6\le x<0.7\\ 0 & 0.7\le x\le 1\end{cases}$$

$$\mu_h(x):\begin{cases}0 & 0\le x\le 0.6\\ x+1 & 0.6<x<0.7\\ 1-x & 0.7\le x<0.8\\ 0 & 0.8\le x\le 1\end{cases},\ \mu_{vh}(x):\begin{cases}0 & 0\le x\le 0.7\\ x+1 & 0.7<x<0.8\\ 1-x & 0.8\le x<0.9\\ 0 & 0.9\le x\le 1\end{cases},$$

$$\mu_{asleep}(x):\begin{cases}0 & 0\le x\le 0.8\\ x+1 & 0.8<x<0.9\\ 1 & 0.9\le x\le 1\end{cases} \qquad (5)$$

The sensitivity function of the above fuzzy rules serves as a criterion for validating the rules (Fig. 16).

The three-dimensional surface illustrates the relationship between the input variables **Eye Aspect Ratio (EAR)** and **Mouth Aspect Ratio (MAR)** and the output variable representing the **degree of drowsiness** in the proposed fuzzy inference system. This surface enables a detailed examination of how the system models individual and joint effects of the two behavioral indicators on the final decision.

The output surface demonstrates that EAR is the most influential variable in determining the drowsiness level. When EAR lies within the range of **0 to approximately 0.2**, the output remains consistently high and close to 1, regardless of the MAR value. This indicates that **eye closure**

strongly activates the fuzzy rules associated with severe drowsiness. As EAR increases beyond **0.35**, the output decreases noticeably and stabilizes between 0.2 and 0.4, reflecting a clear association between open eyes and a low probability of drowsiness. This behavior confirms that the system correctly prioritizes eye-related indicators as primary contributors to drowsiness detection.

The effect of MAR on the output is gradual and exhibits a lower slope compared with EAR. When the eyes are open (high EAR), increasing MAR leads to only a modest increase in the output value. This aligns with physiological patterns, as yawning alone is typically an early or mild indicator of fatigue and does not independently signify a critical drowsiness state. However, in the **intermediate EAR range (approximately 0.25–0.35)**, the influence of MAR becomes more pronounced; higher MAR values result in a substantial increase in the drowsiness output. This behavior highlights the system's ability to capture **the progressive transition from alertness to drowsiness** when both indicators jointly manifest moderate fatigue-related patterns.

The surface reveals a distinct nonlinear interaction between the two inputs. The combination of moderate EAR values with high MAR values produces significantly elevated output levels. This interaction reflects realistic behavioral dynamics, where partial eyelid drooping accompanied by repeated yawning is characteristic of **intermediate or developing stages of drowsiness**. The system's representation of this synergy demonstrates that the fuzzy rule base effectively models the joint contribution of ocular and oral features to the overall assessment.

The presence of step-like transitions in the output surface indicates that the fuzzy system employs **piecewise membership functions and discretized linguistic categories** (e.g., Low, Medium, High). Such discontinuities are typical in Mamdani-type inference systems, where rule boundaries produce clearly defined transitions between different output regions. This structured behavior confirms that the rule set and membership design partition the input space into meaningful regions, enabling the system to provide interpretable and logically consistent responses across varying levels of EAR and MAR.

The analysis of the sensitivity surface demonstrates that:

- EAR is the dominant indicator and strongly modulates the output, especially in regions associated with eye closure.
- MAR exerts a secondary but meaningful influence, particularly in intermediate drowsiness states.
- The fuzzy system captures nonlinear interactions between inputs, reflecting realistic behavioral patterns.
- The stepwise nature of the surface is consistent with the structure of linguistic rules in Mamdani inference.

Overall, the surface confirms that the fuzzy inference system accurately models the complex and progressive characteristics of human drowsiness based on facial behavior.

In the sensitivity plot, the color scheme reflects the degree of drowsiness, with green representing alertness (no drowsiness), yellow indicating moderate drowsiness, and red denoting severe drowsiness.

The driver's drowsiness level was determined using Mamdani inference combined with the centroid method, with the output variable y and its associated membership degree calculated accordingly (Equation 6). Sample values from real-world data used for the calculation and validation of this output are provided in Tables 6 and 7 (Equation 6).

$$y^* = \frac{\sum(\mu(y).y)}{\sum \mu(y)} \quad (6)$$

The inference computations, derived from the sum of weights and the sum of membership functions presented in Tables 6 and 7, are as follows:

$$\begin{cases} \sum(\mu(y).y) = 0.32 + 0.50 + 0.42 = 1.24 \\ \sum \mu(y) = 0.8 + 1.0 + 0.7 = 2.5 \end{cases} \Rightarrow y^* = \frac{1.24}{2.5} = 0.5$$

$$\begin{cases} \sum(\mu(y).y) = 0.36 + 0.63 + 0.80 = 1.79 \\ \sum \mu(y) = 0.6 + 0.9 + 1.0 = 2.5 \end{cases} \Rightarrow y^* = \frac{1.79}{2.5} = 0.7$$

For all values of y within the range [0, 1], the levels of moderate and severe drowsiness are computed using the sum of weights and the sum of membership functions as follows:

$$\begin{cases} \sum(\mu(y).y) = 4.9495 \\ \sum \mu(y) = 9.8990 \end{cases} \Rightarrow y^* = \frac{4.9495}{9.8990} = 0.5$$

$$\begin{cases} \sum(\mu(y).y) = 6.9289 \\ \sum \mu(y) = 9.8990 \end{cases} \Rightarrow y^* = \frac{6.9289}{9.8990} = 0.7$$

Using centroid-based inference, the overall levels of moderate and severe drowsiness are determined as follows:

$$if: \begin{cases} x = Drowsiness \\ y = Level\ Drowsiness \end{cases} \Rightarrow y = \begin{cases} 0, & if\ 0.5 < x < 0.7\ \ (Moderate\ Drowsiness) \\ 1, & if\ x \geq 0.7\ \ (Severe\ Drowsiness) \end{cases}$$

In the output of the Mamdani fuzzy inference system, a value of 0.5 denotes moderate drowsiness, whereas a value of 0.7 corresponds to severe drowsiness. Each individual's drowsiness level is updated and logged in an Excel spreadsheet. For storage, Mamdani output values between 0.5 and below 0.7 are recorded as 0 (moderate drowsiness), while values exceeding 0.7 are recorded as 1 (severe drowsiness). These entries are refreshed with each new test (Fig. 17). The fuzzy membership functions, combined rules, and Mamdani inference outputs are presented in Fig. 18. During drowsiness detection, the values in the table are updated in real time, and the system continuously refreshes the data instantaneously.

3. Results

All trained neural networks, their derived models, and the full image processing and fuzzy logic modules were implemented using Python in the PyCharm environment. Abbreviations are used in this section to streamline the expressions within the summary tables (Table 8). The participants took part in live video testing for an average duration of 5 minutes (ranging from 4 to 6 minutes). Yawning and eye drowsiness were examined. A total of 3,397,500 frames were collected for drowsiness detection. The live videos were fed into the system at a rate of 25 frames per second, and the system used a ResNet50-based deep neural network model to detect drowsiness. Furthermore, a combination of this model with fuzzy inference was employed to determine the level of drowsiness.

Table 9 summarizes the specifications of all neural networks trained for drowsiness detection with two labels: *Normal* and *Drowsiness*. Among them, the ResNet50 network achieved the highest training accuracy, the second-highest validation accuracy, the lowest training error rate, and the third-lowest validation error count. It also outperformed all other networks across test metrics, including training and validation F1-scores, precision, and recall, as well as real-time inference performance. Consequently, ResNet50 was selected as the optimal neural network for distinguishing between Normal and Drowsiness labels.

The ResNet50-derived model, employed for field-testing drowsiness detection, demonstrated real-time processing capability for video frames on an RTX 3060 laptop GPU with 6 GB RAM. A dedicated comparison of all trained models confirmed the superior performance of the ResNet50-based model. The inference models from each network were combined with EAR and MAR image processing techniques and fuzzy logic to both detect drowsiness and quantify its severity. All tests were conducted on an RTX 3060 laptop GPU with 6 GB RAM to evaluate per-frame processing times (Table 10).

An important observation in Table 9 and 10 is that the ViT-Tiny and MobileNetV3 networks, which showed the weakest training performance, achieved the fastest real-time image processing among all models. This outcome is attributed to their poor training results, where lower accuracy translated into faster execution. However, because of their inadequate accuracy, these networks were excluded from the comparative analysis reported in Table 11.

At the conclusion of this section, the ResNet50 neural network is identified as the best-performing model. To further validate its effectiveness, it is compared with related studies conducted by other researchers to assess whether it also surpasses similar approaches (Table 11).

The comparison between the ResNet50 neural network implemented in this study and other related works demonstrated the clear superiority of the model developed in this research. Furthermore, the research gap and the necessity of implementing the proposed method were highlighted in a comprehensive comparison (Table 12).

The field evaluation of the integrated system for drowsiness detection and severity estimation was carried out with 453 volunteers representing diverse Middle Eastern ethnic groups, including Azerbaijani, Gilaki, Mazandarani, Lur, Kurdish, Turkmen, Baluchi, Tajik, Hazara, and Arab. To address the challenge of fluctuating lighting conditions, an infrared camera was employed, allowing the system to automatically switch to infrared illumination when required. Among the 453 trials, 31 errors were recorded, yielding an overall system accuracy of 93.16% (Fig. 19, Table 13). Fuzzy and intelligent approaches for drowsiness detection and related systems were examined in a comprehensive review (Table 14).

Although the accuracy of the combined system is slightly lower than that reported in other similar works (Table 9), those studies did not include large-scale implementation or field testing. In contrast, this study validated its results through extensive evaluation with 453 participants, ensuring the reliability of the findings.

The causes of system errors were documented and analyzed in four distinct scenarios:

- Scenario 1: When a person is shouting, the system may misinterpret it as yawning. In other cases, yawning is detected correctly (Fig. 20-a).
- Scenario 2: Accurate drowsiness detection requires both eyes of the driver to be visible. If not, the system classifies the driver as normal (non-drowsy). In some cases, even face detection and recognition fail (Fig. 20-b).
- Scenario 3: Wearing a face mask prevents the system from recognizing yawning. Since the image is captured from a frontal view, the system attempts to estimate facial landmarks

but cannot determine mouth status. As a result, it defaults to classifying the mouth as closed (normal) (Fig. 20-c).

- Scenario 4: When the driver wears sunglasses, detection accuracy depends on the infrared camera. If IR light passes through and the eyes are visible, detection is correct; otherwise, the system identifies the driver as normal (non-drowsy) (Fig. 20-d).

To further examine the contribution of each component within the proposed architecture, an ablation-style analysis was incorporated into the manuscript. The system was evaluated in three configurations: (1) using the deep neural network alone, (2) using only the EAR/MAR-based fuzzy inference system, and (3) using the full hybrid model. The results indicate that while the ResNet50 model provides highly accurate binary detection, the hybrid model enhances robustness in ambiguous visual conditions and enables reliable estimation of drowsiness severity. Additionally, the comparative analysis section was expanded with transformer-based and state-of-the-art deep learning approaches to provide a more comprehensive performance benchmark. Moreover, a detailed discussion of real-time implementation constraints was added, covering limitations related to GPU dependency, eye occlusion, face masks, IR illumination, head movements, and confusion between yawning and speech. These additions strengthen the scientific rigor of the manuscript and directly address the ablation analysis, benchmarking, and real-time implementation constraints.

This study centers on the implementation of the ResNet50 neural network with a highly practical architecture for training a drowsiness dataset. The network design incorporates convolutional layers with ReLU activation and MaxPooling, followed by a fully connected layer using a sigmoid activation function with two output neurons to maximize classification accuracy for the dataset. The ResNet50 network achieved a training accuracy of 99.74% with minimal errors in both training and validation phases. By integrating the trained model with image processing methods based on EAR and MAR metrics, along with fuzzy logic, a unified system was developed capable of processing video frames in real time. To further assess its ability to determine drowsiness severity, the combined system was tested in field experiments with 453 participants. The results indicated an accuracy of 93.16%, with 31 error cases.

The primary sources of error were identified as: incomplete visibility of both eyes in the image, face masks obscuring the mouth, sunglasses resistant to infrared transmission, and shouting, which interfered with yawning detection.

This reduction mainly arises from uncertainty propagation during fuzzification, threshold-based membership mapping, and the aggregation of multiple inputs to estimate drowsiness intensity rather than performing binary classification alone. Nevertheless, the hybrid CNN–fuzzy framework enables real-time detection along with interpretable estimation of drowsiness levels, enhancing system robustness in practical scenarios. While the CNN-only model achieves higher classification accuracy under controlled conditions, a slight performance reduction is observed after integration with the fuzzy inference system and real-world deployment.

Despite the continuous release of more powerful processors, this study adopted a cost-effective approach by utilizing an RTX 3060 laptop GPU with 6 GB RAM for all training and testing. The proposed system's capabilities can be replicated on similar GPUs, offering real-time, high-accuracy image processing for both detecting and evaluating driver drowsiness. Given its proven accuracy and real-world reliability, the system has strong potential for future integration into in-vehicle image processing units within advanced driver-assistance systems (ADAS).

4. CONCLUSION

The aim of this research was to address aspects overlooked in similar studies, such as conducting field tests with volunteers from diverse ethnic backgrounds, testing under varying lighting conditions, using uniform and cost-effective hardware, and ensuring the practical applicability of the study. All these objectives were addressed through the proposed hybrid approach combining a convolutional neural network and fuzzy inference, offering the added advantage of real-time processing. To maintain real-time processing relationships in the paper when implementing on lower-performance hardware, it is suggested to reduce the number of frames received from the camera. This number should not be set below 10 frames per second. The reason is that if the number of received frames falls below a certain threshold, the system's sensitivity in real-time detection under actual conditions will decrease. While the real-time experiments were conducted on an RTX 3060 GPU, the proposed framework can be adapted for deployment on embedded platforms (e.g., Raspberry Pi) by applying model compression, resolution reduction, or lightweight network variants, albeit with a trade-off in inference speed and accuracy.

ACHNOWLEDGMENT

We extend our appreciation to the students (from various ethnic groups) of the Faculty of Engineering at the Islamic Azad University, YI.C., who voluntarily participated in the field testing of the real-time drowsiness detection image processing system. All participants were fully aware that their facial images would be published in the research article and provided their consent.

References:

[1] H. A. Madni, A. Raza, R. Sehar, N. Thalji and L. Abualigah, **"Novel Transfer Learning Approach for Driver Drowsiness Detection Using Eye Movement Behavior,"** in *IEEE Access*, vol. 12, pp. 64765-64778, 2024, doi: 10.1109/ACCESS.

[2] A. Jarndal, H. Tawfik, A. I. Siam, I. Alsyouf and A. Cheaitou, **"A Real-Time Vision Transformers-Based System for Enhanced Driver Drowsiness Detection and Vehicle Safety,"** in *IEEE Access*, vol. 13, pp. 1790-1803, 2025, doi: 10.1109/ACCESS.2024.3522111.

[3] S. A. El-Nabi *et al.*, **"Driver Drowsiness Detection Using Swin Transformer and Diffusion Models for Robust Image Denoising,"** in *IEEE Access*, vol. 13, pp. 71880-71907, 2025, doi: 10.1109/ACCESS.2025.3561717.

[4] M. Ramzan, A. Abid, M. Fayyaz, T. J. Alahmadi, H. Nobanee and A. Rehman, **"A Novel Hybrid Approach for Driver Drowsiness Detection Using a Custom Deep Learning Model,"** in *IEEE Access*, vol. 12, pp. 126866-126884, 2024, doi: 10.1109/ACCESS.2024.3438617.

[5] F. You, X. Li, Y. Gong, H. Wang and H. Li, **"A Real-time Driving Drowsiness Detection Algorithm with Individual Differences Consideration,"** in *IEEE Access*, vol. 7, pp. 179396-179408, 2019, doi: 10.1109/ACCESS.2019.2958667.

[6] M. Ngxande, J. -R. Tapamo and M. Burke, **"Bias Remediation in Driver Drowsiness Detection Systems Using Generative Adversarial Networks,"** in *IEEE Access*, vol. 8, pp. 55592-55601, 2020, doi: 10.1109/ACCESS.2020.2981912.

[7] M. Venkateswarlu and V. Rami Reddy Ch, **"DrowsyDetectNet: Driver Drowsiness Detection Using Lightweight CNN With Limited Training Data,"** in *IEEE Access*, vol. 12, pp. 110476-110491, 2024, doi: 10.1109/ACCESS.2024.3440585.

[8] S. Priyanka, S. Shanthi, A. Saran Kumar and V. Praveen, **"Data fusion for driver drowsiness recognition: A multimodal perspective,"** in *Egyptian Informatics Journal Access*, vol. 27, 2024, doi: 10.1016/j.eij.2024.100529.

[9] W. Deng and R. Wu, **"Real-Time Driver-Drowsiness Detection System Using Facial Features,"** in *IEEE Access*, vol. 7, pp. 118727-118738, 2019, doi: 10.1109/ACCESS.2019.2936663.

[10] A. Nomura, A. Yoshida, K. Nagumo and A. Nozawa, **"Reducing the effect of face orientation using FaceMesh landmarks in drowsiness estimation based on facial thermal images,"**

in *Springer Nature: Artificial Life and Robotics Access*, vol. 30, pp. 317-324, 2025, doi: 10.1007/s10015-024-01001-1.

[11] H. Lamaazi, A. Alqassab, R. A. Fadul and R. Mizouni, **"Smart Edge-Based Driver Drowsiness Detection in Mobile Crowdsourcing,"** in *IEEE Access*, vol. 11, pp. 21863-21872, 2023, doi: 10.1109/ACCESS.2023.3250834.

[12] D. Salem and M. Waleed, **"Drowsiness detection in real-time via convolutional neural networks and transfer learning,"** in *Journal of Engineering and Applied Science Access*, vol. 71, 2024, doi: 10.1186/s44147-024-00457-z.

[13] Y. Xuan Chew, S. F. Abdul Razak, S. Yogarayan and S. N. M. Sayed Ismail, **"Dual-Modal Drowsiness Detection to Enhance Driver Safety,"** in *Computers, Materials & Continua Access*, vol. 81, pp. 4397-4417, 2024, doi: 10.32604/cmc.2024.056367.

[14] M. Ramzan, H. U. Khan, S. M. Awan, A. Ismail, M. Ilyas and A. Mahmood, **"A Survey on State-of-the-Art Drowsiness Detection Techniques,"** in *IEEE Access*, vol. 7, pp. 61904-61919, 2019, doi: 10.1109/ACCESS.2019.2914373.

[15] V. U. Maheswari, R. Aluvalu, M. P. Kantipudi, K. K. Chennam, K. Kotecha and J. R. Saini, **"Driver Drowsiness Prediction Based on Multiple Aspects Using Image Processing Techniques,"** in *IEEE Access,* vol. 10, pp. 54980-54990, 2022, doi: 10.1109/ACCESS.2022.3176451.

[16] A. Yadav, R. Hussain, M. Shukla, J. B, R. Kalia, S. Prince Mary, C. Hsu, M. K. Mishra, K. Saleem, and M. El-Meligy, **"Enhancing convolutional neural networks in electroencephalogram driver drowsiness detection using human inspired optimizers,"** in *Scientific reports Access*, vol. 15*.* 2025, doi: 10.1109/ACCESS.2022.3187995.

[17] A. Murata, T. Doi and W. Karwowski, **"Sensitivity of PERCLOS70 to Drowsiness Level: Effectiveness of PERCLOS70 to Prevent Crashes Caused by Drowsiness,"** in *IEEE Access*, vol. 10, pp. 70806-70814, 2022, doi: 10.1109/ACCESS.2022.3187995.

[18] J. Cai, X. Liao, J. Bai, Z. Luo, L. Li and J. Bai, **"Face Fatigue Feature Detection Based on Improved D-S Model in Complex Scenes,"** in *IEEE Access*, vol. 11, pp. 101790-101798, 2023, doi: 10.1109/ACCESS.2023.3314665.

[19] A. Z. Mohammed, E. A. Mohammed and A. M. Aaref, **"Real-Time Driver Awareness Detection System,"** in *IOP Conference Series: Materials Science and Engineering Access*, vol. 745, 2020, doi: 10.1088/1757-899X/745/1/012053.

[20] S. Nagdeote, H. Pendhari, M. John and S. Agrawal, **"An Approach to Detect Driver Drowsiness in Real Time using Facial Landmarks,"** in *SAMRIDDHI: A Journal of Physical Sciences, Engineering and Technology Access,* vol. 15, 2023, doi: 10.18090/samriddhi.v15i01.21.

[21] S. Titare, S. Chinchghare and K. N. Hande, **"Driver Drowsiness Detection and Alert System,"** in *International Journal of Scientific Research in Computer Science, Engineering and Information Technology (ISJRCSEIT) Access*, vol. 7, pp: 583-588, 2021, doi: 10.32628/CSEIT2173171.

[22] R. Alshamrani, F. Alshehri and H. Kurdi, **"A Preprocessing Technique for Fast Convex Hull Computation,"** in *Procedia Computer Science Access,* vol. 170, pp. 317-324, 2020, doi: 10.1016/j.procs.2020.03.046.

[23] G. Adarsh, V. Singh, S. Singh and B. Hazela, **"Drowsiness Detection System in Real Time Based on Behavioral Characteristics of Driver using Machine Learning Approach,"** in *Journal of informatics Electrical and Electronics Engineering (JIEEE) Access*, vol. 04, pp. 1-10, 2023, doi: 10.54060/jieee.v4i1.84.

[24] B. Asdyo, B. Kanigoro and Rojali, **"Drowsy Detection System by Facial Landmark and Light Gradient Boosting Machine Method,"** in *Procedia Computer Science Access,* vol. 227, pp. 500-507, 2023, doi: 10.1016/j.procs.2023.10.551.

[25] L. Wang, H. Wang and J. Liu, **"Discrimination of Driver Fatigue Based on Distortion Energy Density Theory and Multiple Physiological Signals,"** in *IEEE Access*, vol. 9, pp. 151824-151833, 2021, doi: 10.1109/ACCESS.2021.3125052.

[26] A. Celecia, K. Figueiredo, M. Vellasco and R. Gonzalez, **"A Portable Fuzzy Driver Drowsiness Estimation System,"** in *Sensors Access*, vol. 20, 2020, doi: 10.3390/s20154093.

[27] M. Arava and D. M. Sundaram, **"Multi-Ftigure Selection and Fuzzy Logic-Based Intelligent Driver Drowsiness Detection,"** in *The Institution of Engineering and Technology (IET) Access*, vol. 19, 2025, doi: 10.1049/ipr2.70052.
[28] W. Alkishri, A. Abualkishik and M. Al-Bahri, **"Enhanced Image Processing and Fuzzy Logic Approach Optimizing Driver Drowsiness Detection,"** in *Applied Computational Intelligence and Soft Computing Access,* vol. 2022, 2022, doi: 10.1155/2022/9551203.
[29] A. Sorourkhah, **"Coping Uncertainty in the Supplier Selection Problem Using a Scenario-Based Approach and Distance Measure on Type-2 Intuitionistic Fuzzy Sets,"** in *Fuzzy Optimization and Modelling Access,* vol. 3, pp. 1-8, 2022, doi: 10.30495/fomj.2022.1953705.1066.
[30] M. A. L. Khaniki, M. B. Hadi and M. Manthouri, **"Tuning of Novel Fractional Order Fuzzy PID Controller for Automatic Voltage Regulator using Grasshopper Optimization Algorithm,"** in *Majlesi Journal of Electrical Engineering Access,* vol. 15, 2012, doi: 10.52547/mjee.15.2.39.
[31] M. Jalali, R. Kardehi and N. Pariz, **"Maximum Energy Absorbed from the Persian Gulf Waves Considering Uncertainty in Power Take off Parameters,"** in *Majlesi Journal of Electrical Engineering Access,* vol. 16, 2022, doi: 10.30486/mjee.2022.696491.
[32] D. N. M. Abadi, A. Moarefianpopur and N. M. Dehkordi, **"Finite-Time Bounded Model-Based Event-Triggered Control for Distributed Fuzzy T-S Systems,"** in *Majlesi Journal of Electrical Engineering Access,* vol. 18, 2024, doi: 10.30486/mjee.2023.1994207.1226.
[33] S. Boulanouar and Fengal Boualem, **"Solar panel fault diagnosis based on the intelligent recursive method,"** in *Majlesi Journal of Electrical Engineering Access,* vol. 19, 2025, doi: 10.57647/j.mjee.2025.1902.28.
[34] N. Z. Janah and B. Baharudin, **"Genetic Fuzzy Filter Based on MAD and ROAD to Remove Mixed Impulse Noise,"** in *Majlesi Journal of Electrical Engineering Access,* vol. 4, 2010, doi: 10.1234mjee.v4i2.283.
[35] S. MR. Soroushmehr, **"A New Fuzzy Based Motion Estimation Algorithm in Video Compression,"** in *Majlesi Journal of Electrical Engineering,* vol. 4, 2010, doi: 10.1234mjee.v4i2.197.
[36] O. D. Ghaleh, V. Maihami and K. Khamforoosh, **"A Hybrid Method for Medical Image Denoising and Segmentation Using Optimized Fuzzy Clustering and Autoencoder,"** in *Fuzzy Optimization and Modeling Journal (FOMJ) Access,* vol. 6, 2025, doi: 10.57647/j.fomj.2025.0602.10.
[37] S. F. Sakhaei, A. J. Afshari, A. Bosaghzade and M. H. M. Jahromi, **"Intelligent Image-Based Recognition of Rice Cultivars Using PSO-Optimized ANFIF,"** in *Fuzzy Optimization and Modeling Journal (FOMJ) Access,* vol. 6, 2025, doi: 10.57647/j.fomj.2025.0603.17.

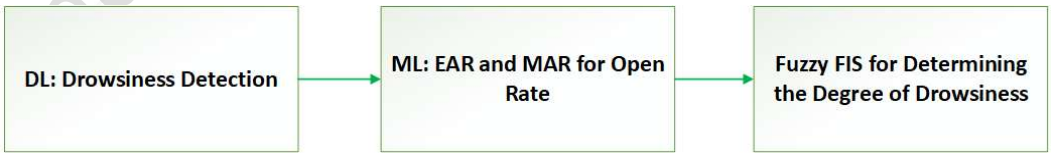

Fig. 1. Overall Block Diagram of the Proposed Architecture.

(a) (b)

Fig. 2 a) Recommended Camera Mounting Location, b) Image Acquired from the Recommended Mounting Position.

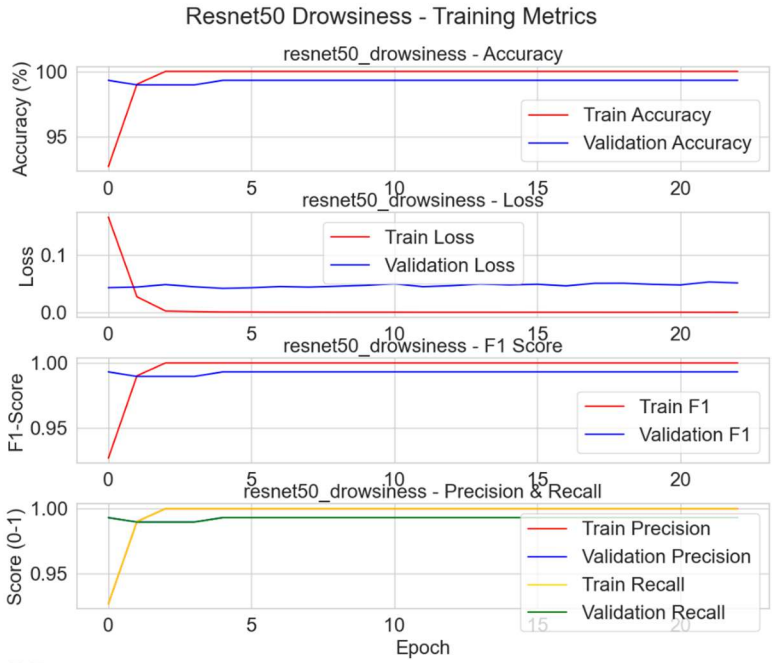

Fig. 3. Training Accuracy and Loss Chart (ResNet50).

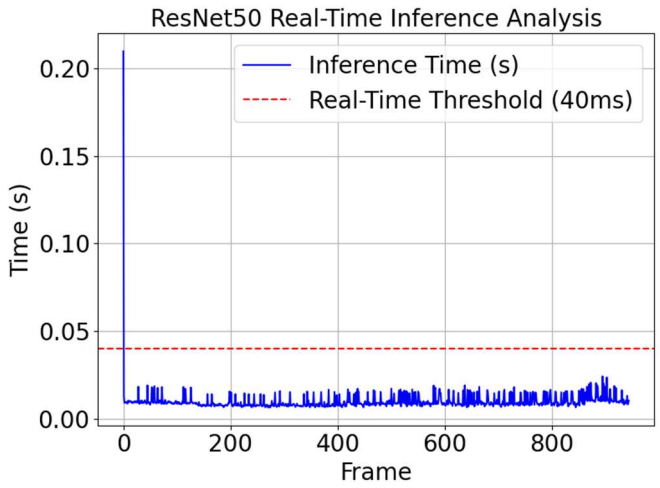

Fig. 4. Real-Time Test Output (ResNet50 Inference).

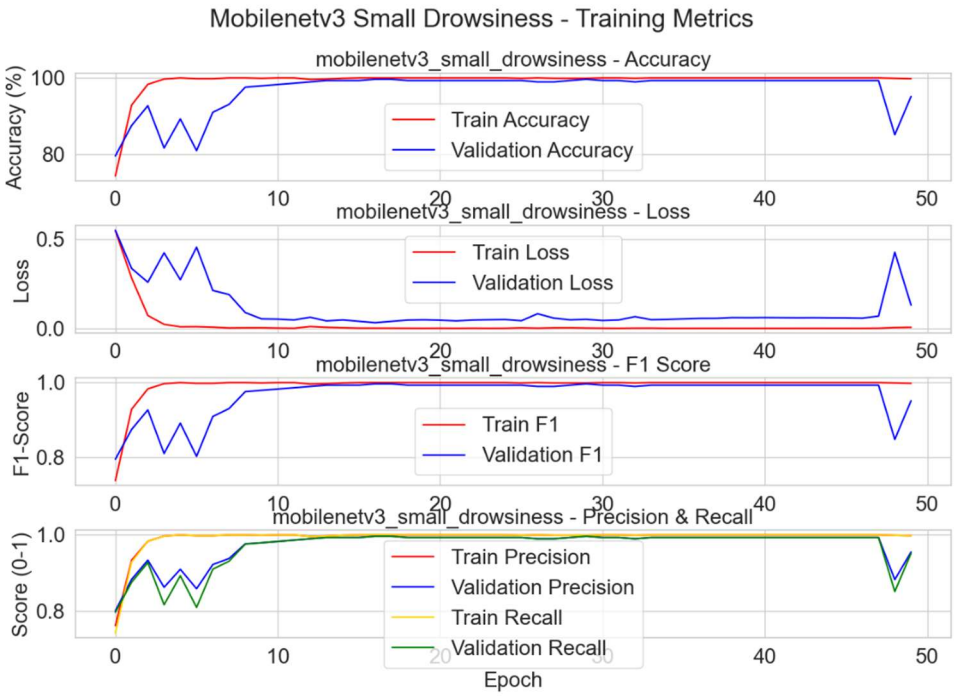

Fig. 5. Training Accuracy and Loss Chart (MobilenetV3).

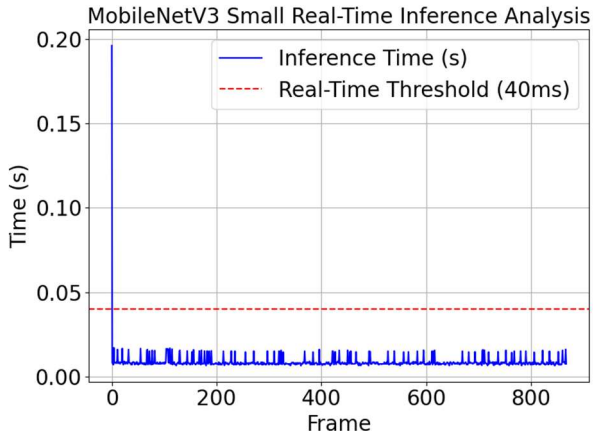

Fig. 6. Real-Time Test Output (MobilenetV3).

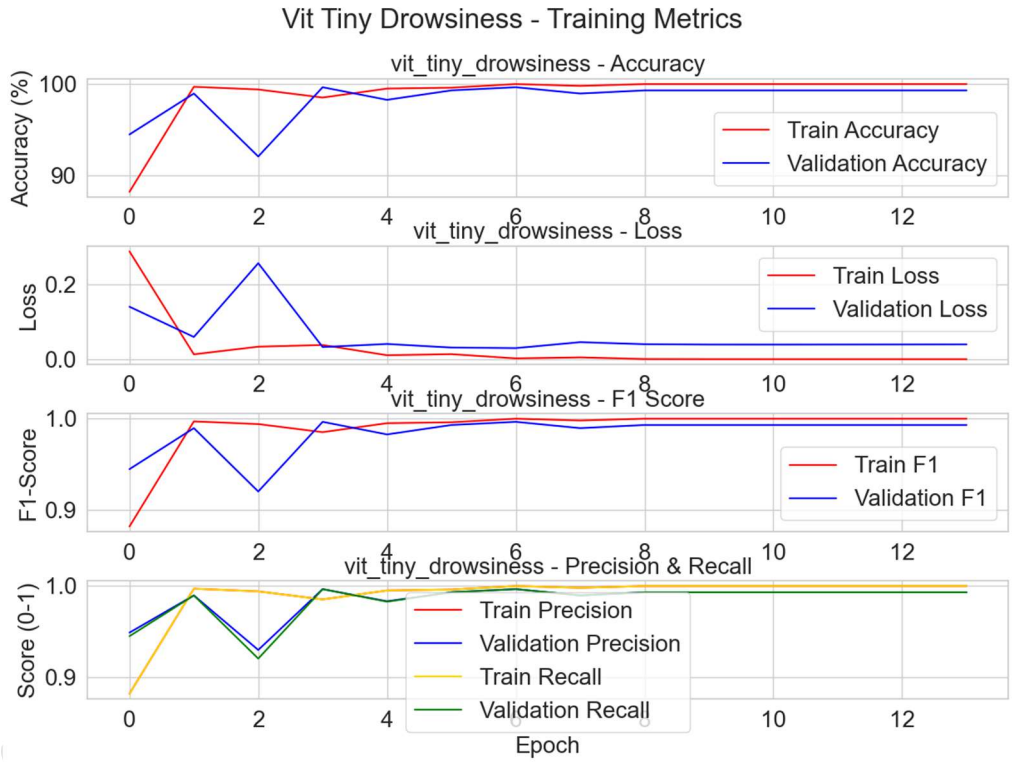

Fig. 7. Training Accuracy and Loss Chart (vit-tiny).

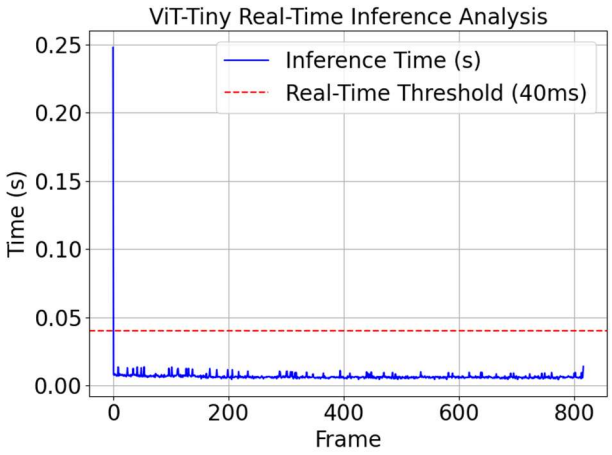

Fig. 8. Real-Time Test Output (vit-tiny).

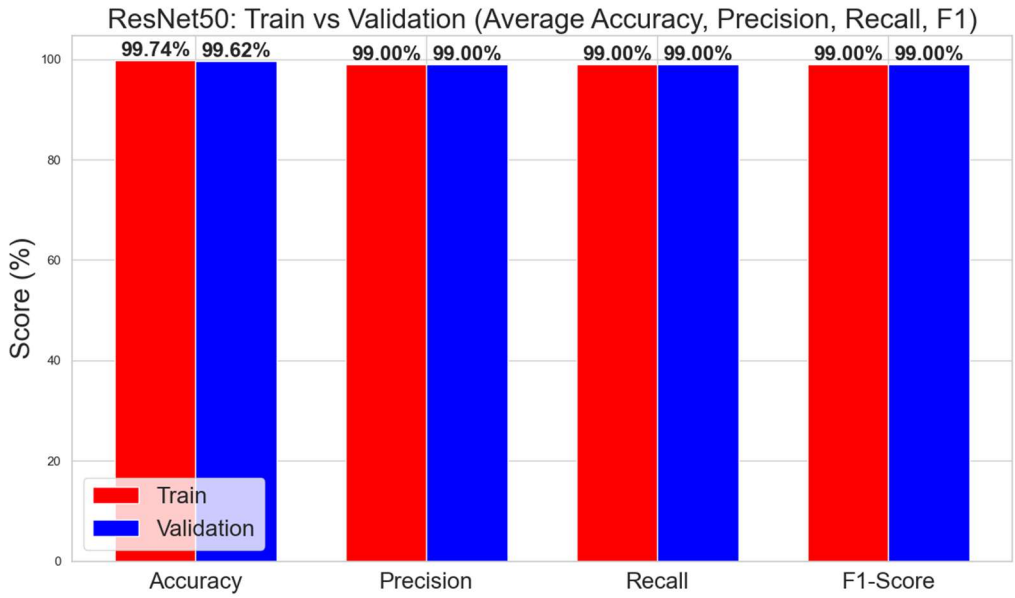

Fig. 9. Comparison of Train and Validation in the ResNet50 Neural Network.

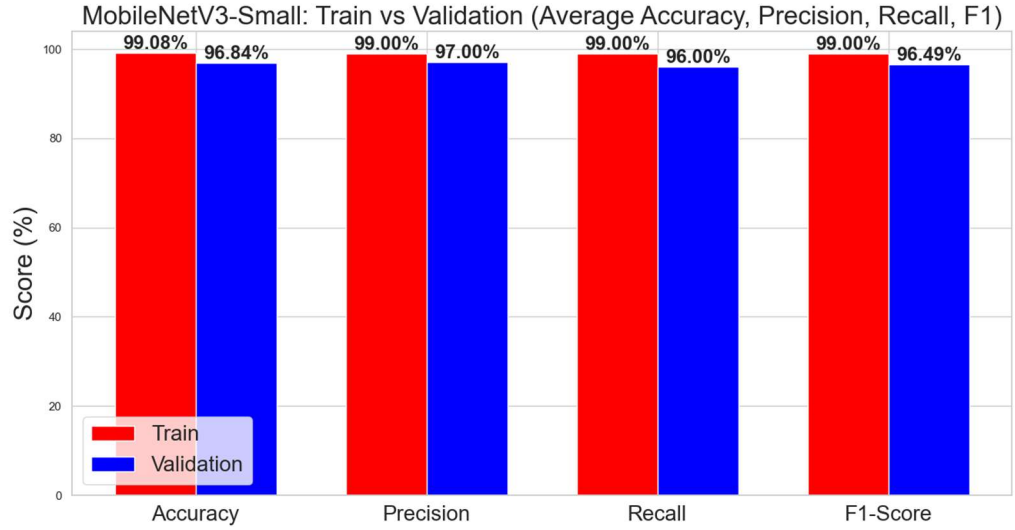

Fig. 10. Comparison of Train and Validation in the MobileNetV3 Neural Network.

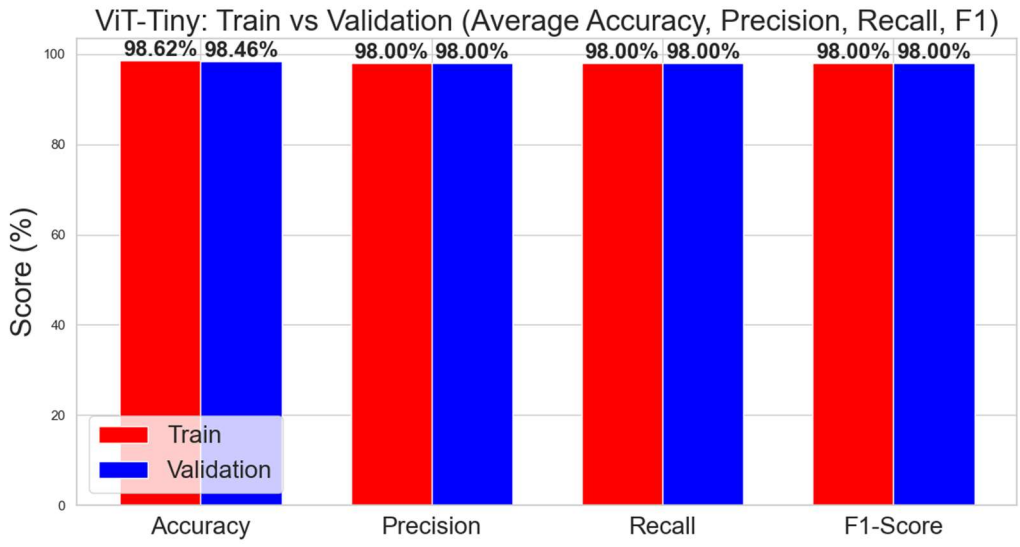

Fig. 11. Comparison of Train and Validation in the ViT-Tiny Neural Network.

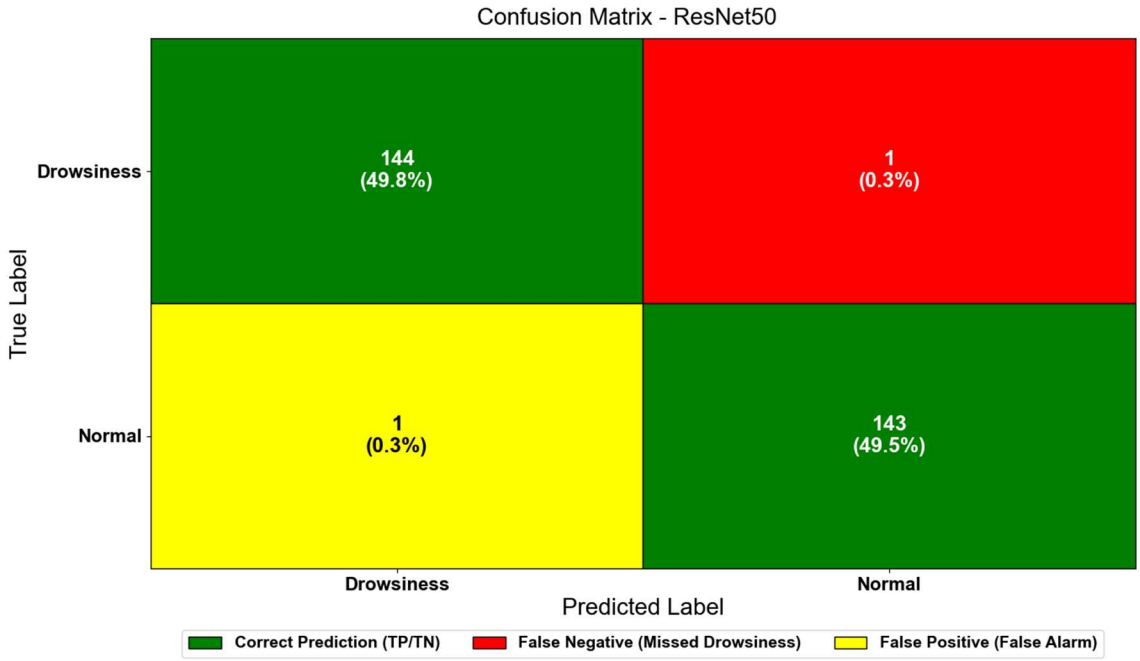

Fig. 12. Confusion matrix for ResNet50.

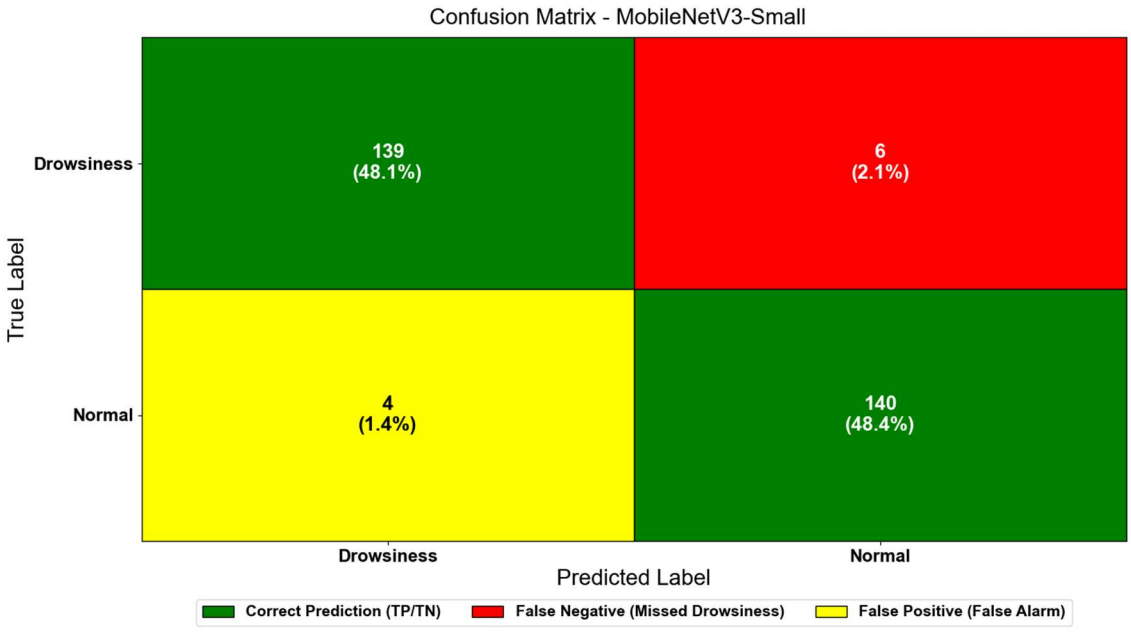

Fig. 13. Confusion matrix for MobileNetV3.

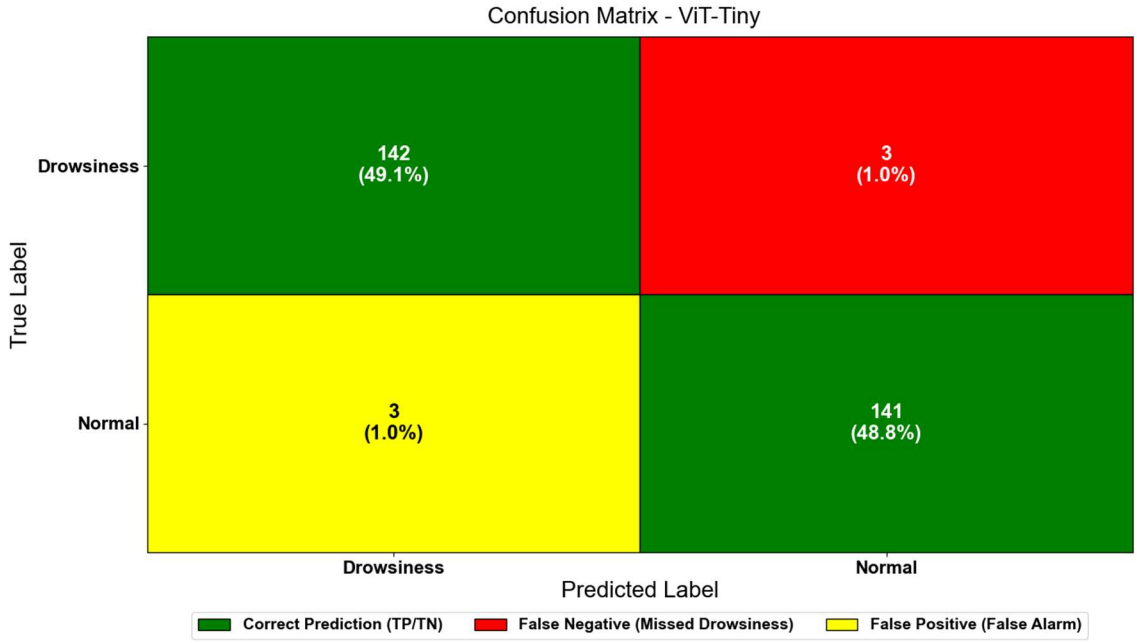

Fig. 14. Confusion matrix for ViT-Tiny.

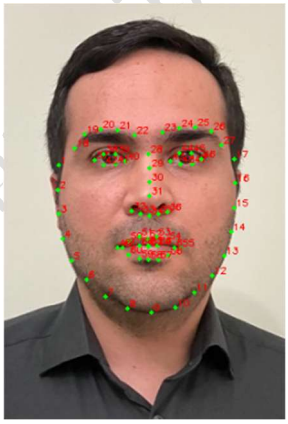

Fig. 15. Detecting 68 facial landmarks.

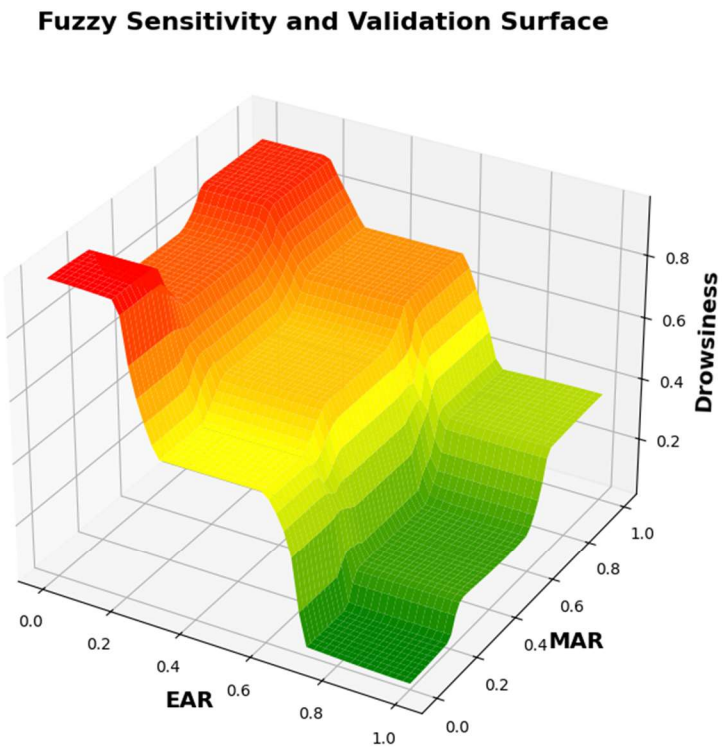

Fig. 16. Fuzzy Sensitivity and Validation Surface.

A
Drowsiness
0
A
Drowsiness
1

Fig. 17. Saving Drowsiness results.

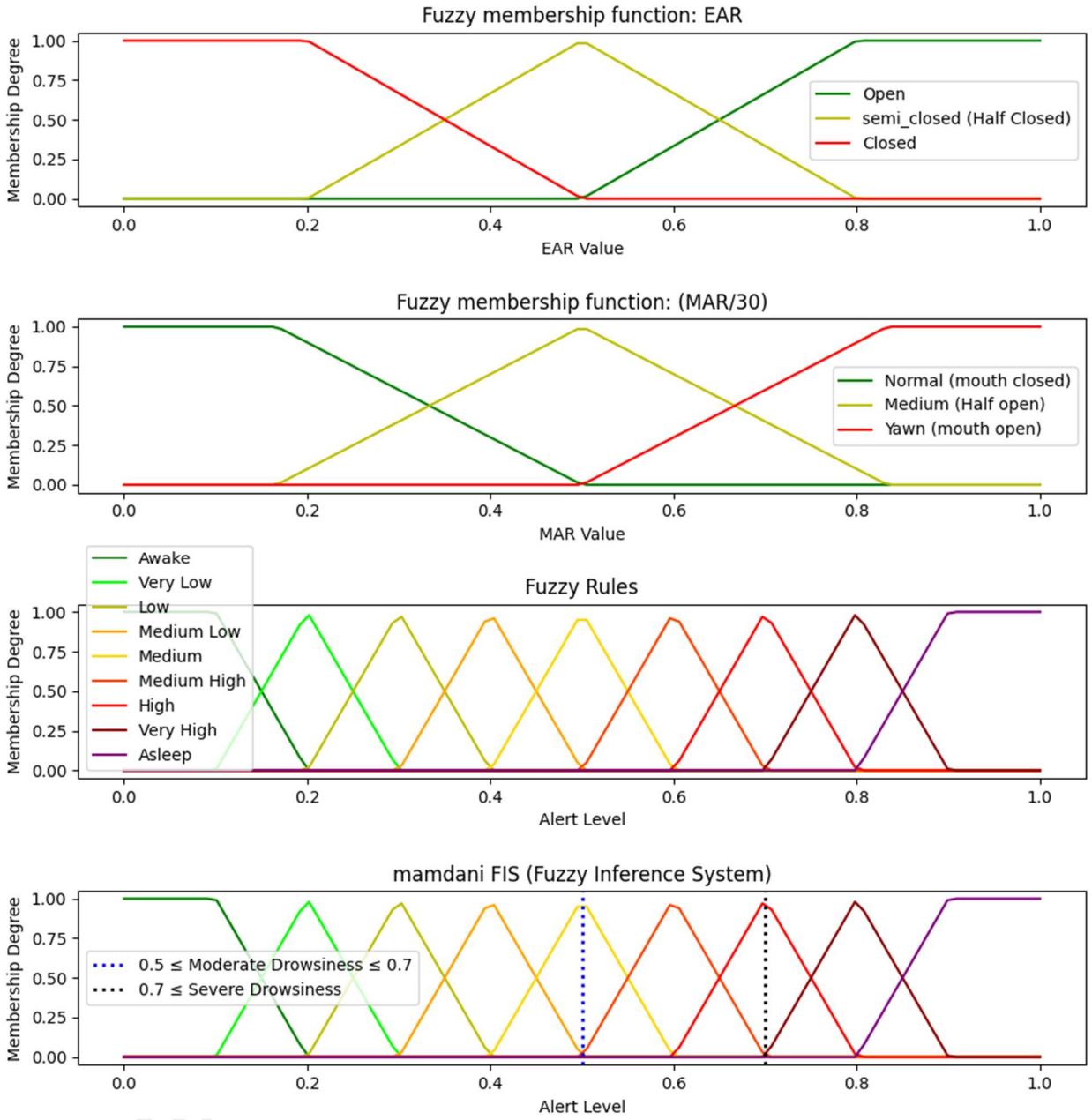

Fig. 18. Membership functions and fuzzy system inference engine in real-time detection of Drowsiness level.

Fig. 19. Examples of Field Tests.

(a) (b) (c) (d)

Fig. 20. Scenario1, 2, 3, 4.

Table 1. Distinctive of the Research.

Distinctive of the Research	Description
Use of the same hardware for training and testing	All neural network training and tests were conducted on the model obtained from extracting the best neural network using the same hardware.
Combining neural network with fuzzy logic	Drowsiness detection accuracy was improved by integrating the model extracted from neural network training with fuzzy logic.
Conducting tests in a real environment with diverse volunteers	The study was performed to obtain real results, including volunteers from different ethnic backgrounds.
Applicability in the automotive industry	The research results can confidently be applied in Advanced Driver Assistance Systems (ADAS).
Addressing identified research gaps	The table explicitly highlights research gaps (e.g., lack of large-scale field validation, limited ethnic diversity in datasets, absence of fuzzy logic integration) and clarifies how our work addresses them.

Table 2. initial settings.

parameters	values
Hardware-GPU	RTX3060-laptop, 6GB of RAM
Real-Time Threshold	0.04 s
Image dimensions in the dataset	640 × 640
Image dimensions during training	224 × 224
Learning-rate	1e-4
Batch-size	32
Num-epochs	50

Table 3. Complete Dataset Specifications.

Feature	Description
Dataset name	Driver Drowsiness Detection (Roboflow, Itomic01)
Total size	1448 images
Number of classes	2 (Normal, Drowsiness)
Class distribution	Number of images labeled as drowsy used for training: 500. Number of images labeled as normal used for training: 513. Number of images labeled as drowsy used for testing: 74. Number of images labeled as normal used for testing: 72. Number of images labeled as drowsy used for validation: 145. Number of images labeled as normal used for validation: 144.
Data splits	Training: 70% (1013 images), Validation: 20% (289 images), Test: 10% (146 images)
preprocessing	All images were resized to 224×224 pixels and converted to tensor format
Data augmentation	No augmentation was applied

Table 4. The parameters configured for the camera capturing the driver's images.

Specification	values
Appearance Type	Bullet
Connection Type	Wired (LAN), Wireless (Wi-Fi)
Image Sensor Type	CMOS
Shutter Speed Range	1/3 s – 1/100,000 s
Supported Resolutions	1080p (1920×1080), 1.3MP (1280×960), 720p (1280×720), VGA (640×480), QVGA (320×240)
Night Vision Capability	Yes
Optical Zoom	×1
Digital Zoom	×16
Viewing Angle	Horizontal: 106°, Vertical: 56°, Diagonal: 135.6° — and also Horizontal: 93°, Vertical: 48°, Diagonal: 114.8°
Minimum Illumination	0.0275 Lux @F2.0 (Color, 80 IRE); 0.0134 Lux @F2.0 (B/W, 80 IRE); 0 Lux (IR on). Also: 0.1983 Lux @F2.0 (Color, 80 IRE); 0.1128 Lux @F2.0 (B/W, 80 IRE); 0 Lux (IR on)
IR Night Vision Details	Smart IR up to 30 meters
Supported Storage	Micro SD up to 256 GB

Table 5. Detecting eyes and mouth.

Name of the detected points	Number of points
Right eye	37-42
Left eye	43-48
The upper line of the upper lip	51-53
Bottom line of the lower lip	57-59
Bottom line of the upper lip	62-64
The upper line of the lower lip	66-68

Table 6. Sample values of moderate drowsiness.

y value	Membership function $\mu(y)$	Product $\mu(y) \times y$
0.4	0.8	0.32
0.5	1.0	0.50
0.6	0.7	0.42

Table 7. Sample values of Severe drowsiness.

y value	Membership function $\mu(y)$	Product $\mu(y) \times y$
0.6	0.6	0.36
0.7	0.9	0.63
0.8	1.0	0.80

Table 8. Abbreviations.

Abbreviation: expression	Abbreviation: expression	Abbreviation: expression
P: Parameters	VP: Validation precision	CHP: CNN + HOG + PCA
TA: Training accuracy (%)	TR: Training recall	DS: DCCNN + SVM
VA: Validation accuracy (%)	VR: Validation recall	SN: Shallow CNN
TL: Training loss	RI: Real-Time inference (s)	CL: CNN-LSTM
VL: Validation loss	R50: ResNet50	MKBY: MC-KFC + blinking + yawning
TF: Training F1-score	M: MobileNetV3	3DF: 3D 478 FFLs (Face Mesh)
VF: Validation F1-score	VT: ViT-Tiny	MN: MobileNet
TP: Training precision	NV: Novel VGLG	R50FF: ResNet50 + Fuzzy FIS

Table 9. Neural Networks Results.

P	R50	M	VT
TA	99.74	99.08	98.62
VA	99.62	96.84	98.46
TL	0.006	0.022	0.034
VL	0.022	0.106	0.077
TF	0.99	0.99	0.98
VF	0.99	0.96	0.98
TP	0.99	0.99	0.98
VP	0.99	0.97	0.98
TR	0.99	0.99	0.98
VR	0.99	0.96	0.98
RI	0.023	0.021	0.021

Table 10. Real-Time Process on RTX3060 laptop GPU.

Inference method	Real-Time (s)
ResNet50 + Fuzzy FIS	0.023
ViT-Tiny + Fuzzy FIS	0.021
MobileNetV3 + Fuzzy FIS	0.021

Table 11. Comparison of Drowsiness Detection Results.

paper	method	TA	recall	precision	TF
[1]	NV	99	0.99	0.99	0.99
[2]	ViT	99.4	-	-	-
[3]	Swin	99.82	-	-	-
[4]	CHP	99.6	0.968	0.597	0.738
[5]	DS	94.8	-	-	-
[6]	GAN	98.01			-
[7]	SN	99.23	1	0.99	0.99
[8]	CL	96	0.95	0.95	0.95
[9]	MKBY	93.6	-	-	-
[10]	3DF	84	-	-	-
[11]	CNN	98.2	0.81	0.92	0.86
[12]	MN	99.94	0.99	0.99	0.99
ours	R50	99.74	0.99	0.99	0.99

Table 12. Comparison of recent studies on driver drowsiness detection with the proposed method.

paper	Year	Method	Dataset	Features/ Modalities	Evaluation Metrics	Main Findings
[1]	2024	Transfer Learning (TL)	Eye movement dataset (proprietary)	Eye Movement behavior	Accuracy, F1	Proposed TL model outperforms baselines in eye-based drowsiness detection
[2]	2025	Vision Transformer (ViT-DDD)	NTHU-DDD, UTA-RLDD	Full-Face image (non-intrusive vision)	Accuracy	ViT-based system achieves 98.89%-99.4%, robust to glasses, sunglasses, lighting changes; resl-time raspberry pi deployment
[3]	2025	Swin Transformer + Diffusion Model	Eye-Blink, CEW	Eye-region images + diffusion denoising	Accuracy, Precision, Recall, F1,	Achieves 99.82%-99.94% accuracy; highly robust to noise & adversarial attacks (FGSM/PGD); diffusion improves visual quality
[4]	2024	Hybrid Deep Learning	Custom dataset	Facial+ behavioral features	Accuracy	Hybrid DL achieves higher accuracy than single CNNs
[5]	2019	Real-time CNN	NTHU-DDD	Facial landmarks+ PERCLOS	Accuracy, ROC	Considers individual differences; good generalization
[6]	2020	GANs for bias reduction	N/A	Facial images	Accuracy	GAN reduces bias in drowsiness detection

[7]	2024	Lightweight CNN (DrowsyDetectNet)	Limited-size dataset	Facial features	Accuracy, Precision	Performs well with small training data
[8]	2024	Data Fusion (multimodal)	Multimodal dataset	EEG+Eye+Video	Accuracy, Recall	Fusion improves recognition compared to single modality
[9]	2019	Real-time CNN	NTHU-DDD	Facial features	Accuracy	Achieves reliable real-time detection
[10]	2025	Thermal + CNN	Thermal face dataset	FaceMesh landmarks	Accuracy	Reduces face orientation effects
[11]	2023	Edge-based ML	Mobile edge dataset	Video+ sensors	Accuracy, Latency	Real-time edge deployment feasible
[12]	2024	TL + CNN	Transfer learning dataset	CNN features	Accuracy	Improves recognition speed
[13]	2024	Dual-Modal Detection	Multimodal dataset	Video+ Physiological	Accuracy, Precision	Improves driver safety with two modalities
[14]	2019	Survey	N/A	Survey	N/A	Comprehensive survey of techniques
[15]	2022	CNN+Multi-aspect Image Processing (EAR, MAR, FAR, gradient-based orientation)	NTHU-DDD, YawDD, EMOCDS, UTA-RLDD	Eye, Mouth, Face, landmarks +Hand gestures + Orientation	Accuracy, TP/TN/FP/FN analysis	Proposed integrated system detects drowsiness from multiple aspects (eye closure, yawning, hand on face, sunglasses, face orientation). Outperforms state-of-the-art methods under varying illumination and scenarios
ours	2025	Hybrid Real-time CNN + Fuzzy	Driver Drowsiness Detection (Roboflow, Itomic01); 453 real test samples	Live camera: CNN features+ Facial landmarks (EAR, MAR)	Accuracy, Precision, Recall, F1-Score	The system demonstrated very high accuracy performance under varying lighting conditions, even with participants from different ethnic backgrounds during the field test.

Table 13. Output Results in Drowsiness Level Detection.

paper	method	Result Accuracy (%)
[25]	NV	95.5
[26]	CHP	97.5
[27]	DS	97.5
[28]	GAN	94.5
Proposed Paper	R50FF	93.16

Table 14. Fuzzy and Intelligent Approaches for Drowsiness & Related Systems.

paper	Year	Application	Method	Contribution
[25]	2019	Driver drowsiness	Fuzzy Inference System	Introduced fuzzy rules for real-time drowsiness
[26]	2020	Driver drowsiness	Portable Fuzzy System	Portable system for fuzzy-based drowsiness
[27]	2025	Driver drowsiness	Multi-feature + Fuzzy Logic	Intelligent fuzzy system for feature selection
[28]	2022	Driver drowsiness	Fuzzy + Image Processing	Enhanced detection via fuzzy optimization
[29]	2019	UAV (Quadrotor)	Sliding Mode + Fuzzy	Improved control via fuzzy-based augmentation
[30]	2012	EMG signals	Adaptive Laguerre + Fuzzy	Eliminates power line noise with fuzzy step-size
[31]	2020	Casting machines	PI + Fuzzy Controller	Hydraulic servo-valve control using fuzzy PI
[32]	2017	Power distribution	Fuzzy DSTATCOM	Power quality improvement
[33]	2025	Solar panels	Recursive + Fuzzy	Fault diagnosis in solar systems
[34]	2014	Clustering	Hybrid GA-PSO + Fuzzy	Automatic clustering optimization
[35]	2010	Video compression	Fuzzy Motion Estimation	Improved motion estimation
[36]	2010	Image denoising	Genetic + Fuzzy filter	Impulse noise removal
[37]	2013	Image processing	Fuzzy Edge Detection	Edge detection in noisy images
ours	2025	Driver drowsiness	Hybrid Real-time CNN+Fuzzy	Combines real-time CNN with fuzzy rules; tested on 453 real-world driver samples for practical accuracy